**ORIGINAL ARTICLE**

# Characterization of the GLONASS-K1+ atomic frequency standard

P. Steigenberger[1] · O. Montenbruck[1]

## Abstract

The fifth GLONASS-K1 satellite with space vehicle number R807 was launched in October 2022. It represents the first spacecraft of the K1+ generation, which offers various technical innovations. Compared to previous K1 satellites, R807 also transmits a code-division multiple access (CDMA) signal in the L2 frequency band in addition to L1 and L2 frequency-division multiple access (FDMA) and L3 CDMA signals. Thus, R807 is the first spacecraft of the K1+ generation. A geometry- and ionosphere-free triple carrier combination is used to analyze the GLONASS R807 clock consistency at different frequencies. Significant inconsistencies were found showing up as variations with a peak-to-peak amplitude of up to 40 cm and periods between 15 min and a few days. Whereas the ultimate explanation for these variations is not known, it is likely that they originate from cross-talk of two oscillators with similar frequency. A short-term clock analysis for integration times up to 100 s based on the one-way carrier phase (OWCP) method shows a superior stability of the R807 clock compared to all other GLONASS satellites including the new K2 generation. The Allan deviation computed from 5 s clock estimates confirms this finding for integration times up to 600 s but shows a significant bump at longer integration times due to the periodic variations mentioned above. Single-frequency OWCP processing confirms consistency of the L1 and L2 FDMA signals whereas the L3 CDMA signal shows a slight phase shift. Although the spurious variations mask the true performance of the K1+ atomic frequency standard, its behavior at short integration times points at a new type of GLONASS satellite clock.

**Keywords** Satellite clock · Triple-carrier combination · Allan deviation · Cross-talk

## Introduction

The Russian global navigation satellite system GLONASS comprises five different generations of satellites (Revnivykh et al. 2017). None of the legacy GLONASS spacecraft launched between 1982 and 2005 is part of the active constellation anymore. Most of the currently operational satellites belong to the modernized GLONASS-M/M+ generations launched between 2005 and 2022. Spacecraft of the K1 and K2 generations are available since 2011 and 2023, respectively. As the first GLONASS-K1 satellite had a different design, this satellite forms a subgroup labeled K1A whereas the currently other three K1 satellites are denoted as K1B (Steigenberger and Montenbruck 2022).

GLONASS satellites are traditionally equipped with cesium (Cs) frequency standards. Compared to other modern GNSS satellite clocks like GPS and BeiDou rubidium (Rb) clocks or Galileo and BeiDou passive hydrogen masers (PHMs), these clocks show a comparatively poor short-term stability. Thus, more stable Rb and PHM clocks were developed for GLONASS in recent years (Gouzhva et al. 1995; Belyaev et al. 2013). Whereas Rb clocks are flown on GLONASS-K1 together with Cs clocks, an additional PHM is hosted on GLONASS-K2 (Revniykh 2024). However, it is currently not confirmed if this PHM was already used as active clock on the first and still the only K2 satellite launched in August 2023.

The Cs clocks of the legacy GLONASS spacecraft were developed by the Russian Institute of Radionavigation and Time in Saint Petersburg (Bauch 2003). A major limitation of these clocks was their limited nominal lifetime of 2 years only (Bassevich et al. 1996). Bassevich et al. (2007) report on four different generations of Cs clocks with increasing stability subsequently installed on the legacy GLONASS satellites. The fourth generation has a frequency stability

✉ P. Steigenberger
  peter.steigenberger@dlr.de

1  Deutsches Zentrum für Luft- und Raumfahrt, German Space Operations Center, D-82234 Weßling, Germany

of $6 \cdot 10^{-14}$ at 1 day and was expected to be used from 2009 onward. As of March 2024, four GLONASS-M satellites with 3rd generation clocks launched in 2007 are part of the active constellation with a nominal frequency stability of $1 \cdot 10^{-13}$ at 1 day. Newer generation GLONASS-K1 satellites have two Cs and two Rb clocks onboard (Mallette et al. 2010). Revnivykh (2012) specifies the expected clock stability with $5 - 10 \cdot 10^{-14}$ for K1 and $1 - 5 \cdot 10^{-14}$ for K2. According to Fatkulin et al. (2012), GLONASS-K2 spacecraft are equipped with two Rb and two Cs clocks as base option. Revniykh (2024) mentions a passive hydrogen maser as additional clock option for K2. This PHM is manufactured by the company Vremya-CH (Belyaev et al. 2013). It has a short-term stability of $7 \cdot 10^{-13}$ at one second and and a long-term stability of $5 \cdot 10^{-15}$ at 1 day. The latter is confirmed by 2-year ground tests conducted by Belyaev et al. (2019). These clocks have an expected operational lifetime of more than 10 years.

Hauschild et al. (2013) analyzed the short-term GNSS clock performance for time periods between one and 1000 s. They report Allen deviations between $2 \cdot 10^{-13}$ and $1 \cdot 10^{-12}$ for GLONASS M+ satellites at integration times of 1000 s. Griggs et al. (2014) also analyzed the short-term GLONASS clock stability but focused on time periods up to 100 s. They only found small differences in stability compared to GPS for integration times exceeding 20 s. However, the Allan deviation for $0.6\,s < \tau < 10$ s was significantly worse than GPS. Griggs et al. (2014) assumed that this degraded performance is caused by the characteristics of the frequency-locked loop synchronizing a crystal oscillator with the Cs frequency standard.

The most recent GLONASS-K1 satellite was launched in October 2022. In the following, it is denoted by its space vehicle number (SVN) R807 assigned by the International GNSS Service (IGS, Johnston et al. 2017). For newer GLONASS satellites, the SVN differs by 100 from the number used by the GLONASS system provider (here 707) to get unique SVNs. R807 signal transmission started on November 3, 2022, with the slot number 25 which is translated to the satellite identifier R25 in the receiver-independent exchange (RINEX) format (Gini 2023). Like all GLONASS satellites, R807 transmits frequency-division multiple access (FDMA) signals in the L1 and L2 frequency bands at 1598.0625–1605.375 MHz and 1242.937–1248.625 MHz, respectively (RISDE 2008). Both bands offer an open service (L1OF, L2OF) as well as a secured service (L1SF, L2SF). Spacecraft of the M+ and K1 generation also transmit an open service code-division multiple access (CDMA) signal at 1202.025 MHz (L3OC, RSS 2016b).

Compared to the four previously launched K1 satellites (R801, R802, R805, R806), R807 transmits an L2 CDMA signal (RSS 2016a) at 1248.06 MHz. This feature identifies

the spacecraft as an updated version named GLONASS-K1+ (Langley 2017). The L2 CDMA signal transmission could be verified with a Javad TRE-3 S receiver located at the German Space Operations Center (GSOC) in Oberpfaffenhofen, Germany. This receiver is equipped with a prototype firmware that supports tracking of L2 CDMA signals as well as L1 CDMA signals, which are currently only transmitted by the first GLONASS-K2 satellite R803.

This study discusses the performance and behavior of the atomic frequency standard of the first GLONASS-K1+ satellite R807. First, the clock consistency is evaluated from triple-frequency carrier phase observations. Periodic variations are identified and analyzed in the time and spectral domain. In the subsequent section, the GLONASS R807 clock stability is assessed. The short-term clock stability is obtained from one-way carrier phase analysis whereas the performance assessment at longer integration times is based on 5 s clock estimates from GNSS network solutions.

## Triple-carrier combination

In this section, the clock consistency of the L1 and L2 FDMA as well as the L3 CDMA signals of R807 is analyzed with a triple-frequency carrier phase observation combination (TCC). This linear combination is geometry- and ionosphere-free and thus reveals frequency-specific effects (Montenbruck et al. 2012). It is the difference of dual-frequency ionosphere-free linear combinations of $L_i/L_j$ and $L_i/L_k$ and can be written as

$$
\begin{aligned}
\text{TCC}_{i,j,k} =& \left( \frac{f_i}{f_i^2 - f_j^2} - \frac{f_i}{f_i^2 - f_k^2} \right) \cdot L_i \\
&- \frac{f_j}{f_i^2 - f_j^2} \cdot L_j + \frac{f_k}{f_i^2 - f_k^2} \cdot L_k
\end{aligned}
\tag{1}
$$

where $i$, $j$, and $k$ are frequency indices for the three different carriers L.

Twelve globally distributed stations equipped with Septentrio PolaRx5 or PolaRx5 TR receivers from the GNSS tracking networks of the IGS (Johnston et al. 2017) and the Plate Boundary Observatory (UNAVCO Community 2007) have been used to obtain continuous time series of the TCC. L1OF ($L_i$), L2OF ($L_j$) and L3OC pilot observations ($L_k$) served as input for Eq. (1). Passes of individual stations have been aligned w.r.t. each other. The R807 TCC time series of January 20, 2024, is given in Fig. 1. Pronounced periodic variations with an amplitude of about 10 cm and a period of roughly 2 hours are clearly visible.

To get an impression of the stability or possible variations of the TCC oscillations with time, Fig. 2 shows the daily TCC
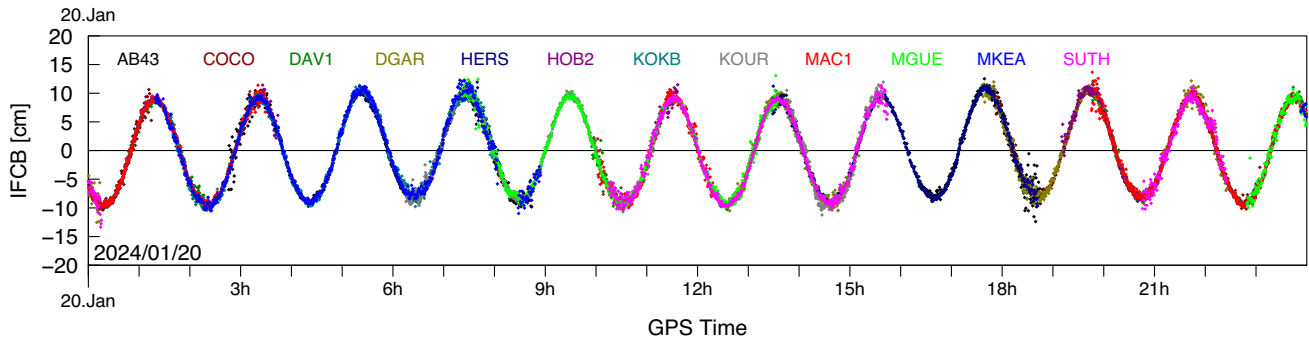
**Fig. 1** Triple-carrier combination of GLONASS R807 L1OF, L2OF, and L3OC signals for 12 stations on January 20, 2024

as color-coded heat map for the time period from November 23, 2022 until February 9, 2024. Transmission outages of all or individual signals are indicated by white color and described by the footnotes of Fig. 2. This figure shows that the TCC periodicity is not constant but extends over a wide frequency range. These frequencies vary gradually but can also change abruptly, mostly after transmission outages. For the period from February 7, 2023 until March 22, 2023, a significantly increased frequency of the TCC oscillations can be observed. A frequency of about 100 cycles per day (cpd) corresponding to a period of 15 min can be read from the spectrogram in Fig. 3. From the end of April until November 2023, the TCC only shows low-frequency variations with periods of one to two days. Starting in November 2023, the frequency slowly rises to 4 cpd and then rapidly increases to about 12 cpd during the first days of January 2024.

Based on the analysis of triple-frequency carrier phases, Montenbruck et al. (2012) have earlier identified apparent clock variations with a similar amplitude for the GPS Block IIF satellites. In this case, the respective variations are synchronized with the orbital period and their amplitude depends on the elevation of the Sun above the orbital plane, which points at a thermal origin.

For R807, the observed TCC variations are obviously not related to the GLONASS orbit period of 11 h, 16 min. Instead, they might originate from cross-talk of oscillators with slightly different frequencies. Oscillator cross-talk has previously been observed in the timing systems of, e.g., the Galileo IOV-1/2 and Sentinel-3A satellites. It manifests in a periodic variation of the resulting clock signal with a beat frequency equal to the frequency difference of the two oscillators and an amplitude proportional to the coupling of the interfering clock. Based on a phasor model (Booker 1965), Montenbruck et al. (2015) derived the expression

$$\delta\rho(t) = \alpha \cdot A \cdot \sin\left(2\pi \cdot \delta f \cdot t + \delta\phi_0\right) \quad \text{with} \quad A = \frac{c}{2\pi f_0} \quad (2)$$

for the periodic range variation caused by mixing of a primary clock signal of frequency $f_0$ with a secondary signal of

frequency $f_0 + \delta f$. Here, $\alpha \ll 1$ denotes the cross-coupling factor, i.e., the amplitude ratio of the two signals. The initial phase offset is $\delta\phi_0$ and $c$ denotes the vacuum speed of light. In the case of GLONASS with a master oscillator frequency $f_0$ of 5.115 MHz, $A$ amounts to 9.3 m. For the maximum observed amplitude of about 20 cm, a cross-coupling factor $\alpha$ of approximately 0.02 is obtained.

A similar cross-coupling was found for the first two Galileo IOV satellites E101 and E102 (Montenbruck et al. 2015). However, the cross-coupling factor of about $0.5 \cdot 10^{-3}$ and the corresponding amplitudes of 2–3 mm are significantly smaller, whereas the beat frequency of about 6 Hz is much higher. For E101 and E102, Montenbruck et al. (2015) attributed the cross-talk to an interference in the clock monitoring and control unit.

In the case of R807, the apparent clock variations show periods with a minimum of about 15 min corresponding to a maximum beat frequency $\delta f$ of about 1 mHz. It appears unlikely that two physically independent atomic frequency standards onboard the GLONASS satellite would provide a frequency consistency at the $10^{-10}$ level or better, so a coupling of clocks from distinct signals can probably be excluded. Unless the problems were related to the design of the K1+ frequency standard itself, it might relate to the coupling of the master clock signal to the navigation signal generation unit. This might explain phase shifts in the periodic variation of L1/L2 FDMA and L3 CDMA carrier phases, even though the detailed interference mechanism is not understood and the actual cause of the apparent clock errors remains unknown.

## Clock stability

Irrespective of the periodic variations described in the previous section, the short-term stability of GNSS satellite clocks can be evaluated by the so-called one-way carrier phase (OWCP) method (Gonzalez and Waller 2007; Delporte et al. 2010). Here, the GNSS receiver tracking the

**Fig. 2** Heatmap of the L1OF/L2OF/L3OC triple-carrier combination of R807. [a] 2 h transmission outage, [b] 2.5 h transmission outage, [c] Transmission outage, [d] L3 transmission outage, [e] PRN switch R25 → R26, [f] PRN switch R26 → R25, [g] Transmission outages
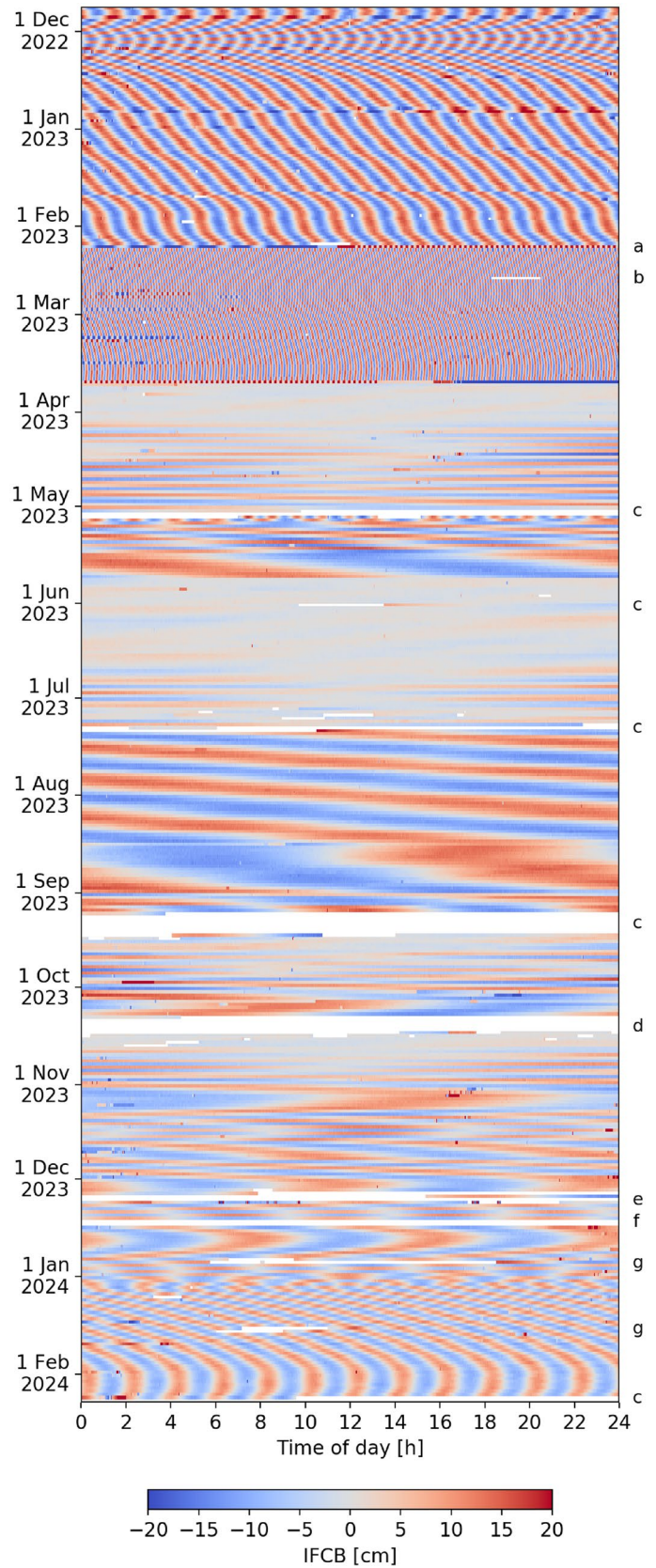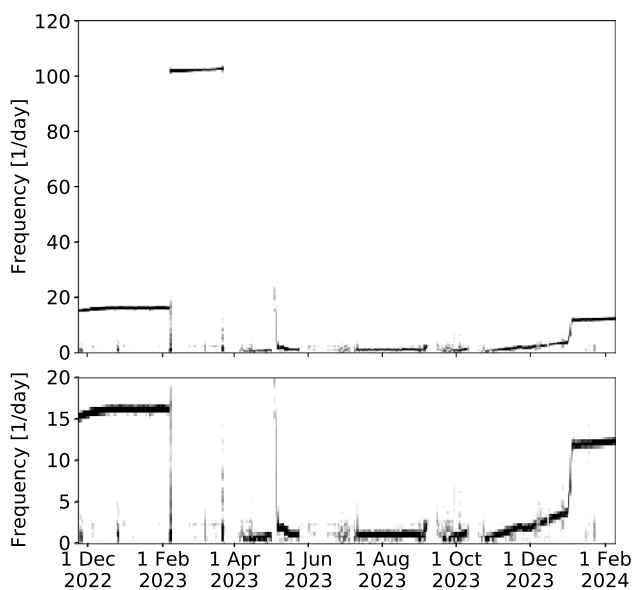
**Fig. 3** Spectrogram of the triple-carrier combination of R807. The lower plot provides a zoom into the upper plot



**Fig. 4** Representative example of short-term Allan deviations of GLONASS satellites obtained from L1OF one-way carrier phase analysis of the IGS station CEBR00ESP. The K1+ satellite R807 is highlighted by a bold line

satellite of interest is connected to a highly stable clock, usually a hydrogen maser. Thus, the impact of the receiver clock on detrended phase residuals can be neglected. The geometry between receiver and satellite antenna is modeled by precise station coordinates and satellite orbits. Remaining effects like the impact of the ionosphere and troposphere, the receiver clock drift as well as ambiguities and phase biases are removed by a low-order polynomial. Remaining effects are primarily the satellite clock, short-period atmospheric variations as well as noise and multipath. The latter can be minimized by using only observations with high elevation angles.

Figure 4 shows an example for the GLONASS short-term clock stability represented by the overlapping Allan deviation (ADEV, Allan 1987) for all active GLONASS satellites on January 28, 2024. The clock analysis is based on the OWCP approach with L1 single-frequency 1 Hz observation data of a GNSS receiver at the IGS station CEBR00ESP in Cebreros, Spain. Time periods for individual satellites have been selected by their highest elevation angle. The precision of the ADEV values determined by this method is on a level of $\sigma(\log \text{ADEV}) \approx 0.1$ evaluated by the results of consecutive days as well different stations. Compared to the legacy GLONASS-M, the M+ satellites show a slightly better stability. The K1B clocks have an improved stability at very short integration times up to 10 s but do not outperform the M+ clocks at integration times longer than 400 s. The K2 clock shows slightly better stability compared to M/M+/K1B. Whereas K2 shows the best stability for integration times up to 2 s, the GLONASS-K1+ clock of R807 shows
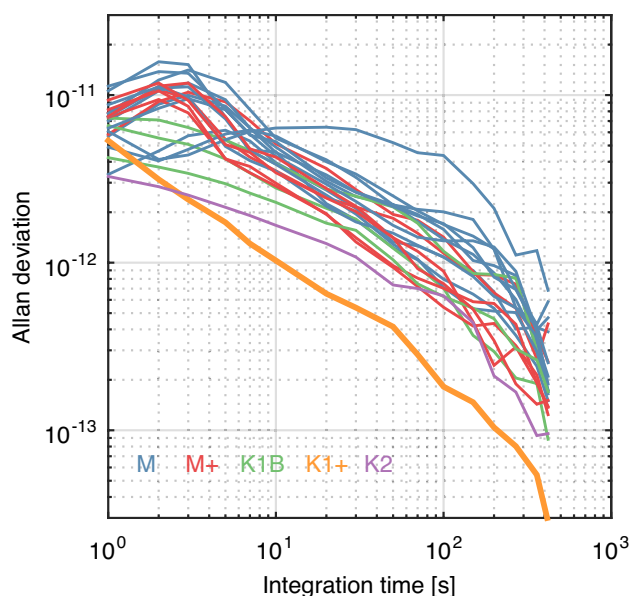
the best stability for longer integration times with an ADEV of $1 \cdot 10^{-12}$ at 10 s and $2 \cdot 10^{-13}$ at 100 s.

The Allan deviation at longer integration times is given in Fig. 5. It was obtained from a one-week data arc of 5 s clock
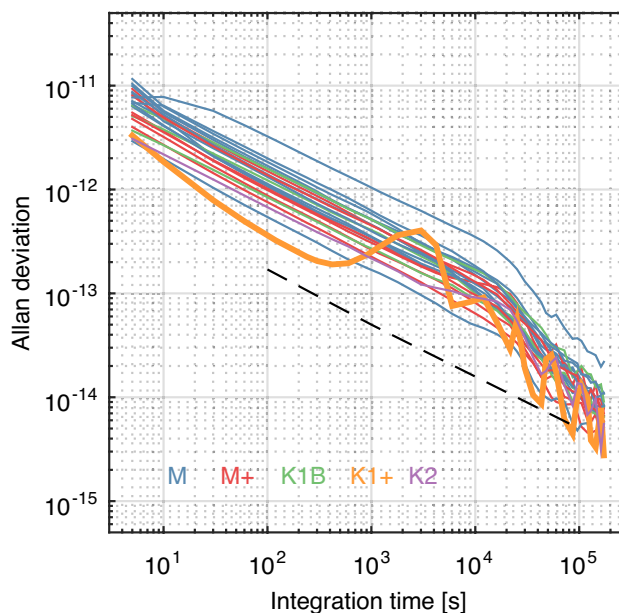


**Fig. 5** Allan deviation of GLONASS satellites for GPS week 2299 obtained from CODE 5 s ionosphere-free L1/L2 clock products. The K1+ satellite R807 is highlighted by a bold line. The straight dashed line shows the specification of the K2 PHM as given in Revnivykh (2016)
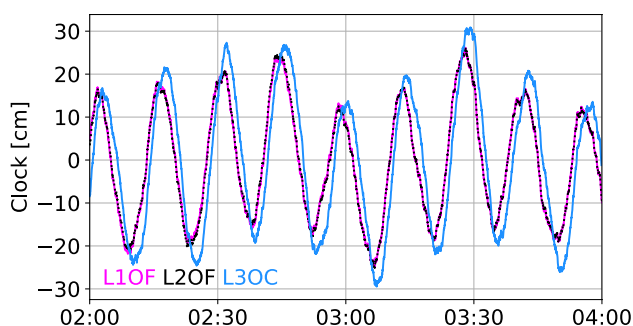
**Fig. 6** One-way carrier phase clock estimates of the IGS station CEBR00ESP on February 21, 2023

estimates of the Center for Orbit Determination in Europe (CODE, Dach et al. 2023). In the absence of detailed information on the clock types used on individual GLONASS satellites, only a general trend towards higher clock stability on the recently launched M+ satellites may be noticed, indicating the use of Rb clocks. For K1B satellites, the average clock stability appears similar to the GLONASS-M satellites suggesting that most K1B satellites are presently operated with a Cs frequency standard. As an exception, R807 shows the lowest overall ADEV for periods between 10 and 600 s. The bump at 3000 s is caused by the periodic clock variations already discussed above and reflects a clock beat period of about 6000 s at that time. Nevertheless, the ADEV minima at integer multiples of the clock beat frequency indicate the performance of the physical clock that also outperforms the other satellites at longer integration times.

According to Revnivykh (2016), the Allan deviation of the K2 (originally denoted as "enhanced GLONASS-K") passive hydrogen maser can be described by $2 \cdot 10^{-12}/\sqrt{\tau[\,s]}$ for integration times $100\,\mathrm{s} < \tau < 1,00,000\,\mathrm{s}$. This ADEV is illustrated by a dashed line in Fig. 5. The enhanced performance provides a clear indication that the currently active atomic frequency standard of R807 represents a new generation of onboard clocks even though the observed performance is slightly lower than expected for the new hydrogen maser.

For further analysis, clock time series for the individual L1OF, L2OF, and L3OC signals obtained from single-frequency OWCP for February 21, 2023, are shown in Fig. 6. The selected date falls into the six-week time interval with 15 min periodicity in spring 2023 (Fig. 2). Here, the OWCP method can be safely applied while longer periods encountered at other times of the year cannot be reasonably covered. The periodic variations exhibit a peak-to-peak amplitude of about 40 cm for all three frequencies. Surprisingly, the L1OF and L2OF estimates are strictly in phase and of equal amplitude, while the L3OC values show a slight phase shift and increased amplitude. This suggests that the FDMA and CDMA navigation signal generation units are either driven

by two distinct effective signals or are themselves responsible for the observed clock interference. The L1/L2 clock differences range from −1.2 to 1.7 cm with an STD of 0.5 cm whereas the L1/L3 differences range from −12.3 to 13.4 cm due to the phase offset. Due to the different amplitude and phase of the L3OC clock variation relative to L1OF and L2OF, the geometry- and ionosphere-free TCC likewise exhibits an oscillation with the same base period and non-zero amplitude as illustrated in Fig. 1.

## Summary

The first K1+ satellite R807 shows an improved clock performance compared to other satellites of the GLONASS constellation. However, the apparent clock stability is degraded by periodic clock variations with periods between 15 min and a few days. Changes in the frequency of the clock variations are largely associated with transmission outages indicating maintenance work onboard the satellite. The apparent clock variations are likely caused by cross-talk of two oscillators with slightly different frequencies although the exact mechanism remains unknown. Nevertheless, the improved stability of the K1+ atomic frequency standard at short integration times points at a new type of GLONASS clock, maybe a passive hydrogen maser, although this assumption is also unconfirmed and the expected performance of the K2 PHM is not met.

As of early 2024, R807 is still set unhealthy. Nevertheless, it is included in the precise orbit and clock products of various IGS analysis centers. For GLONASS, these products are based on the ionosphere-free linear combination of L1 and L2 FDMA observations. Despite its periodic clock variations, precise point positioning (PPP, Zumberge et al. 1997) users can fully exploit R807 in their applications as long as they use high-rate clock products requiring no or only short-term interpolation as well as the same observation types. At the current stage, it is not clear if further satellites of the GLONASS-K1+ generation will be launched or if R807 is a single prototype satellite like GLONASS-K1A. Clock analysis of future K1 as well as K2 satellites will contribute to a better understanding of the employed frequency standards.

**Author contributions** PS performed the data analysis and prepared the initial manuscript. Both authors contributed to the discussion and interpretation of results and critically reviewed the final manuscript.

## Declarations

**Conflict of interest** The authors have no Conflict of interest that are relevant to the content of this article.

**Ethical approval and consent to participate** Not applicable.

## References

Allan D (1987) Time and frequency (time-domain) characterization, estimation, and prediction of precision clocks and oscillators. IEEE Trans Ultrason Ferroelectr Freq Control 34(6):647–654

Bassevich AB, Bogdanov PP, Gevorkyan AG, Tyulyakov AE (1996) GLONASS onboard time/frequency standards: Ten years of operation. In: Proceedings of the 28th Annual Precise Time and Time Interval Systems and Applications Meeting. Reston, Virginia, pp 455 – 462

Bassevich A, Shebshaevich B, Tyulyakov A, Zholnerov V (2007) Onboard atomic clocks GLONASS: current status and future plans. In: Proc ION GNSS 2007, Fort Worth, Texas

Bauch A (2003) Caesium atomic clocks: function, performance and applications. Meas Sci Technol 14(8):1159–1173. https://doi.org/10.1088/0957-0233/14/8/301

Belyaev AA, Demidov NA, Medvedev SY, Pavlenko YK, Sakharov BA, Vorontsov VG (2019) Russian hydrogen masers for ground and space applications. In: 2019 URSI Asia-Pacific Radio Science Conference (AP-RASC), IEEE. https://doi.org/10.23919/ursiaprasc.2019.8738340

Belyaev A, Biriukov A, Demidov N, Likhacheva L, Medvedev S, Myasnikov A, Pavlenko Y, Sakharov B, Smirnov P, Storojev E, Tulyakov A (2013) Russian hydrogen masers for space applications. In: Proc ION PTTI 2013:87–93

Booker HG (1965) A vector approach to oscillations. Academic Press, New York and London

Dach R, Schaer S, Arnold D, Brockmann E, Kalarus MS, Prange L, Stebler P, Jäggi A (2023) CODE final product series for the IGS. https://doi.org/10.48350/185744.

Delporte J, Boulanger C, Mercier F (2010) Simple methods for the estimation of the short-term stability of GNSS on-board clocks. In: Proceedings of the 42nd Annual Precise Time and Time Interval Meeting. Reston, Virginia, pp 215–223

Fatkulin R, Kossenko V, Storozhev S, Zvonar V, Chebotarev V (2012) GLONASS space segment: satellite constellation, Glonass-M and Glonass-K spacecraft main features. In: Proc ION GNSS 2012. Nashville, Tennessee, pp 3912–3930

Gini F (2023) RINEX, The receiver independent exchange format, Version 4.01. Tech. rep., IGS/RTCM. https://files.igs.org/pub/data/format/rinex_4.01.pdf

Gonzalez F, Waller P (2007) Short term GNSS clock characterization using one-way carrier phase. In: 2007 IEEE International Frequency Control Symposium Joint with the 21st European Frequency and Time Forum. IEEE, pp 517–522. https://doi.org/10.1109/freq.2007.4319127

Gouzhva Y, Gevorkyan A, Myasnikov A, Kryukov G, Gankin V, Kornishov O, Teplova S (1995) Activities of the Russian Institute of Radionavigation and Time in development of GLONASS onboard Q-enhanced oscillating compact H-maser. In: Proceedings of the 1995 IEEE International Frequency Control Symposium (49th Annual Symposium), IEEE, FREQ-95. https://doi.org/10.1109/freq.1995.483894

Griggs E, Kursinski ER, Akos D (2014) An investigation of GNSS atomic clock behavior at short time intervals. GPS Solut 18(3):443–452. https://doi.org/10.1007/s10291-013-0343-7

Hauschild A, Montenbruck O, Steigenberger P (2013) Short-term analysis of GNSS clocks. GPS Solut 17(3):295–307. https://doi.org/10.1007/s10291-012-0278-4

Johnston G, Riddell A, Hausler G (2017) The International GNSS Service. In: Teunissen P, Montenbruck O (eds) Springer Handbook of Global Navigation Satellite Systems, chap 33. Springer, pp 967–982. https://doi.org/10.1007/978-3-319-42928-1_33

Langley RB (2017) Innovation: GLONASS—past, present and future. GPS World 28(11):44–49

Mallette L, White J, Rochat P (2010) Space qualified frequency sources (clocks) for current and future GNSS applications. Proc IEEE/ION PLANS 2010:903–908. https://doi.org/10.1109/PLANS.2010.5507225

Montenbruck O, Hugentobler U, Dach R, Steigenberger P, Hauschild A (2012) Apparent clock variations of the Block IIF-1 (SVN62) GPS satellite. GPS Solut 16(3):303–313. https://doi.org/10.1007/s10291-011-0232-x

Montenbruck O, Hauschild A, Häberling S, Braun B, Katsigianni G, Hugentobler U (2015) High-rate clock variations of the Galileo IOV-1/2 satellites and their impact on carrier tracking by geodetic receivers. GPS Solut 21(1):43–52. https://doi.org/10.1007/s10291-015-0503-z

Revnivykh I (2016) GLONASS program update. In: 11th Meeting of the International Committee on Global Navigation Satellite Systems. https://www.unoosa.org/pdf/icg/2016/icg11/01.pdf

Revnivykh S (2012) Main results of the past GLONASS program. objectives and tasks of the new federal program of GLONASS sustainment, development and use. In: Proc ION GNSS 2012, GLONASS Workshop, Nashville, Tennessee

Revnivykh S, Bolkunov A, Serdyukov A, Montenbruck O (2017) GLONASS. In: Teunissen P, Montenbruck O (eds) Springer Handbook of Global Navigation Satellite Systems, chap 8. Springer, pp 219–245. https://doi.org/10.1007/978-3-319-42928-1_8

Revnivykh I (2024) GLONASS status. In: Workshop on GNSS for Policy and Decision Makers, UTokyo/ICG. https://home.csis.u-tokyo.ac.jp/~dinesh/GNSS_Train_files/202402/PresentationMaterials/A04_GLONASS.pdf

RISDE (2008) GLONASS interface control document: Navigation radiosignals in bands L1, L2; version 5.1. Russian Institute of Space Device Engineering

RSS (2016) GLONASS interface control document: Code division multiple access open service navigation signal in L2 frequency band, 1.0. Russian Space Systems, JSC

RSS (2016) GLONASS interface control document: Code division multiple access open service navigation signal in L3 frequency band, 1.0. Russian Space Systems, JSC

Steigenberger P, Montenbruck O (2022) IGS satellite metadata file description, Version 1.00, December 13, 2022. Tech. rep. https://doi.org/10.57677/metadata-sinex

UNAVCO Community (2007) PBO GPS network—AB43-CapeSpenceAK2007 P.S., The GAGE Facility operated by EarthScope Consortium, GPS/GNSS observations dataset. https://doi.org/10.7283/T5SF2T6T

Zumberge JF, Heflin MB, Jefferson DC, Watkins MM, Webb FH (1997) Precise point positioning for the efficient and robust analysis of GPS data from large networks. J Geophys Res 102(B3):5005–5017. https://doi.org/10.1029/96JB03860

**Peter Steigenberger** received his master and PhD degrees in Geodesy from Technische Universität München (TUM) in 2002 and 2009, respectively. Currently, he is senior researcher at DLR's German Space Operations Center (GSOC). His research interests focus on GNSS data analysis, in particular precise orbit and clock determination of GNSS satellites and the evolving navigation systems Galileo, BeiDou, and QZSS.

**Oliver Montenbruck** is head of the GNSS Technology and Navigation Group at DLR's German Space Operations Center, where he started work as a flight dynamics analyst in 1987. His current research activities comprise space-borne GNSS receiver technology, autonomous navigation systems, spacecraft formation flying, precise orbit determination, and multi-constellation GNSS.